climate

MDPI

Review

Understanding the Recent Global Surface Warming Slowdown: A Review

Ka-Kit Tung [1,*] and Xianyao Chen [2,3]

[1] Department of Applied Mathematics, University of Washington, Seattle, WA 98195, USA
[2] Key Laboratory of Physical Oceanography, Ocean University of China, Qingdao 266100, China; chenxy@ouc.edu.cn
[3] Qingdao National Laboratory of Marine Science and Technology, Qingdao 266100, China
* Correspondence: ktung@uw.edu; Tel.: +1-206-685-3794

Received: 1 June 2018; Accepted: 19 October 2018; Published: 24 October 2018

Abstract: The Intergovernmental Panel on Climate Change (IPCC) noted a recent 15-year period (1998–2012) when the rate of surface global warming was a factor of 4 smaller than the mean of the state-of-art climate model projections and than that observed in the previous three decades. When updated to include 2014 by Karl et al. using the new version of NOAA data, the observed warming trend is higher, but is still half or less, depending on dataset used, that of previous decades and the multi-model mean projections. This period is called a surface warming slowdown. Intense community efforts devoted to understanding this puzzling phenomenon—puzzling because atmospheric greenhouse gas accumulation has not abated while surface warming slowed—have yielded insights on our climate system, and this may be an opportune time to take stock of what we have learned. Proposed explanations differ on whether it is forced by counteracting agents (such as volcanic and pollution aerosols and stratospheric water vapor) or is an internal variability, and if the latter, on which ocean basin is responsible (Pacific, Indian, or Atlantic Ocean). Here we critically review the observational records, their analyses and interpretations, and offer interpretations of model simulations, with emphasis on sorting through the rather confusing signals at the ocean's surface, and reconciling them with the subsurface signals.

Keywords: global warming slowdown; hiatus; IPO; trade wind intensification; AMOC; AMO

1. Introduction

1.1. Was There a Hiatus, or a Slowdown?

IPCC's Fifth Assessment Report (AR5) [1] noted "a much smaller increasing trend" of 0.05 °C per decade of the global-mean surface temperature over the 15-year period 1998–2012, than the previous 30 to 60 years. This period, when the least-squares linear trend of surface temperature is close to zero, has been referred to as the "hiatus" or "pause" in surface warming. When updated to 2014 [2], a record warm year, it may be more appropriately called a "slowdown", especially when the latest data from National Oceanic and Atmospheric Administration (NOAA) revised this trend upward. The terminology, "surface warming slowdown" has now been adopted for that period by the US CLIVAR panel [3].

Figure 1 is an updated version of the figure in AR5 using the latest version of the four observational products up to the end of 2017. Much of the change in the linear trend is due to the addition of 2013 and 2014. While the NOAA dataset has the largest increase in 2014 among the ones examined, it nevertheless falls within the observational uncertainty given by the Hadley Centre and so is not qualitatively different from the other datasets. The figure shows that the observed global-mean surface

temperature, including its error bars, remains near the lower bound of the projected warming by the 42 climate models assessed by IPCC, and significantly below the multi-model mean, up to 2014. It then changed in 2015–2016, an extreme El Niño year, when the observed warming caught up to the multi-model mean projection, before declining in 2017.

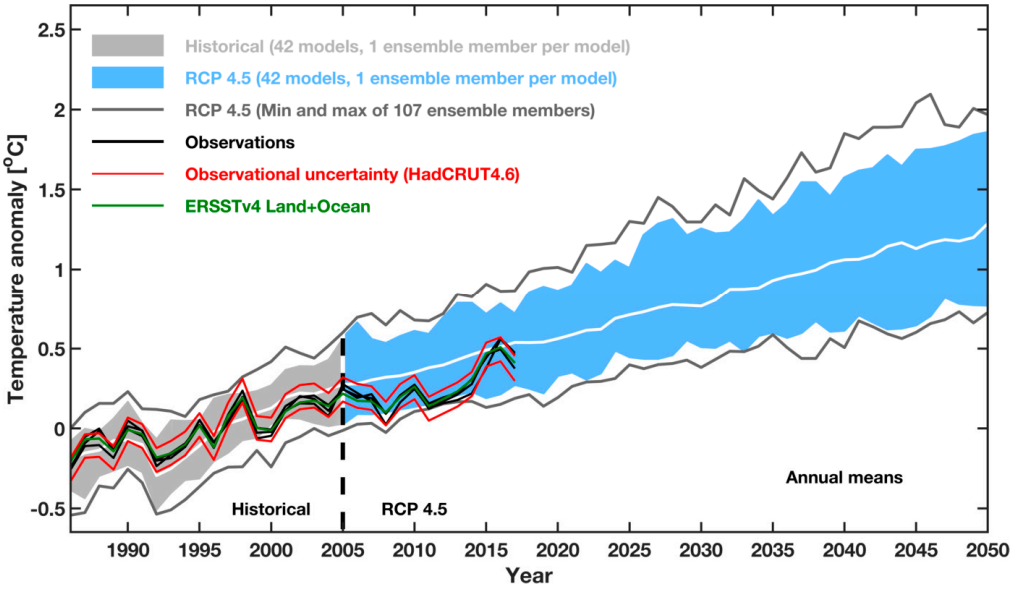

Figure 1. Modeled and observed annual-mean global-mean surface temperature relative to 1986–2005 mean. Adapted from IPCC AR5 Figure 11.9 and updated to the end of 2017. The observations from HadCRUT4.3 [4], GISTEMP [5] and ERA-Interim [6] are in black lines and NCDC (ERSST.v4 land + ocean) is in green. GISTEMP uses ERSST.v4 SST [2] for its sea-surface temperature (SST). The red line is the one standard deviation of combined observational uncertainty due to measurement, sampling and coverage. The shading shows the 5–95% range of 42 models, with grey for the historical simulation and blue for the projection under the RCP4.5 scenario. The white line is for the multi-model mean. The grey curves are the maximum and minimum envelopes of 107 ensemble members.

1.2. How Long Has the Slowdown Lasted?

This period of global-warming slowdown was bracketed by the strong El Niño events of 1997–1998 and 2015–2016. These interannual variations may not be relevant to the decadal and interdecadal phenomenon that we are interested in, and yet they prominently influence the determination of the linear trends and popular perceptions on the start and end dates of this phenomenon. The interdecadal and multidecadal behavior can be better revealed a few hundred meters under the ocean surface, since interannual surface variations tend to have shallow subsurface manifestations.

Which ocean should we look at to find the subsurface signal? It is reasonable to look at the ocean basin that contributes most to the slowdown in the global-mean surface temperature. As reviewed in Section 2, and in Chen and Tung [7], the variation of the global-mean surface temperature at decadal and interdecadal time scales is contributed mostly by an Atlantic pattern. The Pacific's contribution to the global mean surface temperature variation is mostly at the interannual scales (specifically the interannual El Niño-Southern Oscillation (ENSO) timescales). Its contribution at decadal and longer timescales is small and was found to be one order of magnitude smaller than that by the Atlantic [7]. The Atlantic Meridional Overturning Circulation (AMOC) is strongly implicated as the cause of the change in sea-surface temperature in the form of Atlantic Multidecadal Oscillation (AMO) in models [8–11]. In a recent publication on observational evidence of AMOC's variation and its effect on the global-mean surface temperature, Chen and Tung [9] examined the subsurface change associated with variation of AMOC in the recent decades. The acceleration of AMOC started in 1993, reaching a peak in 2005. Then it declined, and will soon reach the previous low level, 26 years later.

Chen and Tung [12] argued that a period of rapid warming may resume and that period may last over two decades. During AMOC's accelerating phase before 2005, deep convection increased and more heat was transported downward in the subpolar Atlantic. The heat that was transported into the deeper layers was sequestered, depriving the surface of the heat that would have warmed it. Unlike the preindustrial era, however, the surface still warms for a while because of the presence of greenhouse heating even though some of the heating is sequestered in the oceans. It took 6 years for the ocean sequestration to overcome the addition of heat from above, until 1999, for the surface to experience a noticeable slowdown in global warming.

Figure 2 shows the coincidence of such heat and salinity subduction in the subpolar Atlantic with the period of surface warming slowdown and acceleration.

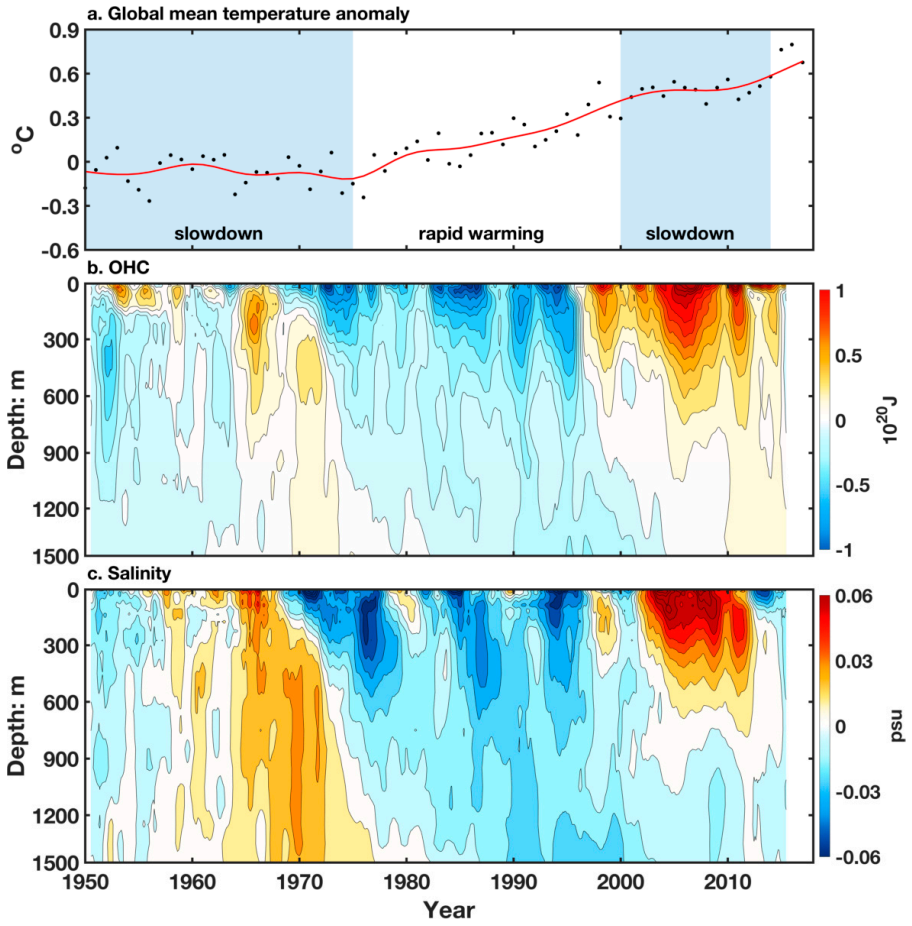

Figure 2. Coincidence of the three AMOC phases with global warming slowdown and acceleration: (**a**) Global mean surface temperature; (**b**) OHC north of 45° N in the Atlantic; (**c**): Salinity north of 45° N in the Atlantic. Adapted and updated to the end of 2017 from Chen and Tung [12].

Atlantic was not the only ocean that was sequestering heat during this period. The subsurface ocean heat content in the Southern Ocean was observed to increase at least since 1993. We will show in Section 3 that while the Pacific and the Indian Oceans dominate the horizontal exchanges of heat in the upper 300 m, the Atlantic and the Southern Ocean dominate the vertical redistribution. They accounted for about 70% of the global heat storage increase in the 200–1500 m layer during 2000–2014, divided between the North Atlantic, which is dominant before 2005, and the Southern Ocean after 2005. The subsurface warming in the Southern Ocean started at least since 1993, and was attributed to the southward displacement and intensification of the circumpolar jet [13], caused in large part by the Antarctic ozone hole [14]. North Atlantic's role appears to be cyclic on decadal timescales, with AMOC in an accelerating phase before 2005.

2. Looking for Clues at the Surface

2.1. Contributions to the Global-Mean Surface Temperature Variation

The relevant question seems to be: what caused the low-frequency variability that has contributed to the alternating periods of global-mean warming acceleration and slowdown? Figure 3a shows the observed global average of the HadCRUT4.3 land + ocean surface temperature [4,15] (in black) and its smoothed version (in blue). It is seen that the global-warming slowdown in the 21st century and the prior hiatus in mid-20th century exist in the smoothed data, with interannual fluctuations (green) superimposed upon the smoothed, multidecadally varying, platform. The high-frequency fluctuation is mostly associated with ENSO, as its associated spatial pattern is the cold-tongue pattern in the equatorial Pacific, seen in Figure 3d. Zhang et al. [16] and Chen and Wallace [17] emphasized that equatorial wave dynamics (Kelvin waves and Rossby waves) are mainly responsible for the interannual "ENSO cycle", with a spectral peak of ~2–7 years and the tight cold-tongue shape near the equatorial Pacific. The spatial pattern associated with the secular trend (Figure 3b), on the other hand, has the typical pattern of anthropogenic forced warming, with more uniformed warming over the globe, but warmer continents than over oceans, and with a characteristic cool "warming hole" in the North Atlantic [18].

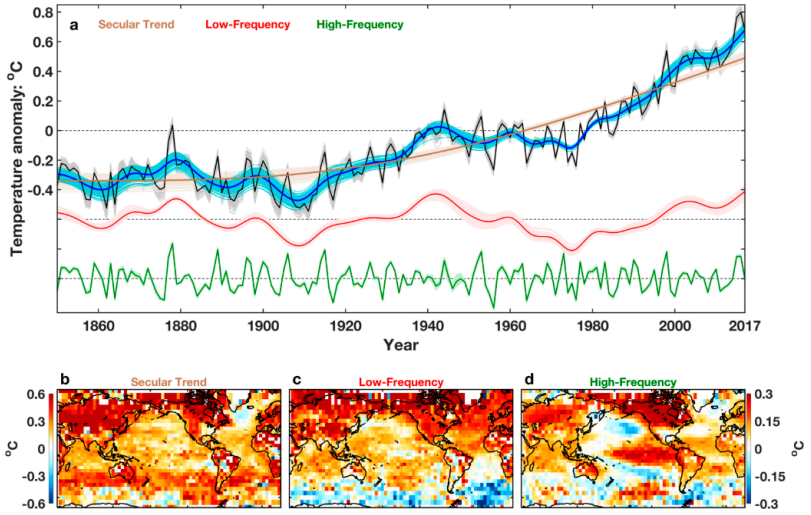

Figure 3. Decomposition of the annual-mean global-mean temperature (relative to 1961–1990 mean): One hundred ensemble members in the HadCRUT4.3 dataset, sampling systematic components of observational uncertainty, are shown in light grey. Their ensemble mean is in black. (**a**) Decomposition of each of the ensemble members of the HadCRUT4.3 global-mean surface (land+ocean) temperature into its high-frequency (shorter than decadal; in green) and low-frequency (longer than decadal, in red) components. The secular trend is indicated with the brown line. The blue lines, which are the sum of the red and the brown lines, are seen as a good smoothed version of the original time series. The darker color line denotes the ensemble mean of the light color lines. The method used in the decomposition is Ensemble Empirical Mode Decomposition [19] (EEMD), which has the advantage that it is lossless (the three components add up to the original time series perfectly) and that the high and low frequency components are constructed to be orthogonal (for all practical purposes in the implementation). The high-frequency component can also be seen as the difference between the original data and the smoothed version. Bottom panels: Spatial patterns obtained by regressing the global land+ocean surface temperature for the period 1910–2014 onto the secular trend (brown curve) (**b**) onto the low-frequency component (the red curve) (**c**) and the high-frequency component (the green curve) (**d**) after the low and high frequency time series are first normalized to unit standard deviation, so that the color shows the amplitude in degrees C. The left color scale is for the secular trend, while the right color scale is for the low and high frequency oscillations. Adapted and updated from Chen and Tung [7] to the end of 2017.

To explain the warming slowdown in the global-mean surface temperature, one needs to explain the low-frequency (period longer than decadal) part of that time series—the associated spatial pattern is shown in Figure 3c—but not necessarily the high-frequency ENSO-cycle fluctuations on top of it. The same procedure was previously used by Wu et al. [20] in finding the spatial SST pattern in the multidecadal mode with an average period of 65 years, except that here we broaden the frequency range to include the decadal variability in order to examine the recent period of slowed warming. The SST pattern is dominated by the inter-hemispheric dipole, called the Atlantic Multidecadal oscillation (AMO), in the Atlantic basin [11,20–24], being warm in the North Atlantic but cool in the South Atlantic and vice versa; this much discussed pattern is known to reflect the subsurface variation of the AMOC [9,22,25]: The upper branch of AMOC is north flowing in both hemispheres, bringing warm tropical surface water to the subpolar North Atlantic, making it warmer, and cold Antarctic surface water northward, making the tropics and midlatitudes of the South Atlantic cooler. This inter-hemispheric pattern is strengthened when AMOC speeds up and weakened when it slows down, giving rise to the alternating anomaly pattern of the multidecadal variability in the Atlantic basin seen in Figure 3c. The Pacific extension (likely through the atmospheric bridge [9]) of this low-frequency pattern in Figure 3c is very weak in comparison and is consistent with the view that interdecadal components of ENSO should fall in the red-noise continuum of the spectrum [26,27]. It is also consistent with the result of Chen and Tung [7] that the Pacific Decadal Oscillation contributes very little to the global-mean surface temperature (see Figure 8 later) variation at decadal and interdecadal timescales. In our decomposition shown in Figure 3, the high- and low-frequency components are orthogonal and so it avoids the problem of the high variance ENSO pattern (Figure 3d) leaking into the Pacific portion of Figure 3c and giving rise to an "ENSO-like" spatial pattern in the low frequencies.

Booth et al. [28] were able to simulate the multidecadal component of the global-mean temperature as a forced response to anthropogenic time-varying aerosol forcing incorporating enhanced indirect aerosol effects. However, since aerosol loading exists in the Northern Hemisphere in both the Atlantic and Pacific, it appears inconsistent with the spatial pattern shown in Figure 3c, which is dominant only in the Atlantic. More importantly, Zhang et al. [29] pointed out that the simulated subsurface behavior from aerosol forcing is different than the observed one, the latter being characteristic of an internal variability caused by variations of AMOC. This mutidecadal quasi–periodic signal was also found in long preindustrial records [11,30–33] and control climate model runs without anthropogenic forcing changes [34–37].

2.2. Trade-Wind Intensification in the Tropical Pacific

A large number of papers—to be reviewed below—argued instead that it is the cooling in the Pacific Ocean that is responsible for the global-warming slowdown. However, simultaneous with the cooling trend in the eastern equatorial Pacific [38,39] for 1997–2014 a compensating warming trend in the western and northern part of the Pacific is also observed (Figure 4). The underlying cause of the compensating trends of the eastern and western Pacific is probably the intensifying trade wind, which blows from east to west, as pointed out by England et al. [39], Han et al. [40] and Delworth et al. [41]. Its effect is seen in the unprecedented sea-level rise in the western Pacific and the lowering of sea level in the eastern Pacific [42,43]. Several authors suggested that the tropical Pacific's trade wind intensification was driven by SST warming in neighboring basins, by the Indian Ocean [40,44], or by the Atlantic Ocean [25,45,46]. The recent work of Lee et al. [47] argued that the warming of the Indian Ocean is not a cause but an effect, as the intensified trade wind drove warm surface waters from the western Pacific into the Indian Ocean through the Indonesian Through Flow (ITF). Clement et al. [48] had long predicted the strengthening trade winds and La Niña-type SST as a consequence of global warming via the mechanism of "oceanic thermostat", which they claimed was not adequately modeled in the current climate models. Evidence supporting their theory from the past 130 years of anthropogenic warming had been weak [49], but could the predicted situation finally emerged in the Pacific in the recent two decades? And could this be the reason why the Climate Model

Intercomparison Project version 5 (CMIP5) models are all, with the exception of one [50], too warm in the eastern equatorial Pacific compared with observation [51]? Whatever its course, this multidecadal behavior did not impact the global mean because it serves mostly to move the warm surface water from the eastern equatorial Pacific to the western and northern Pacific. The mean SST of the Pacific as a whole actually has a slight warming trend.

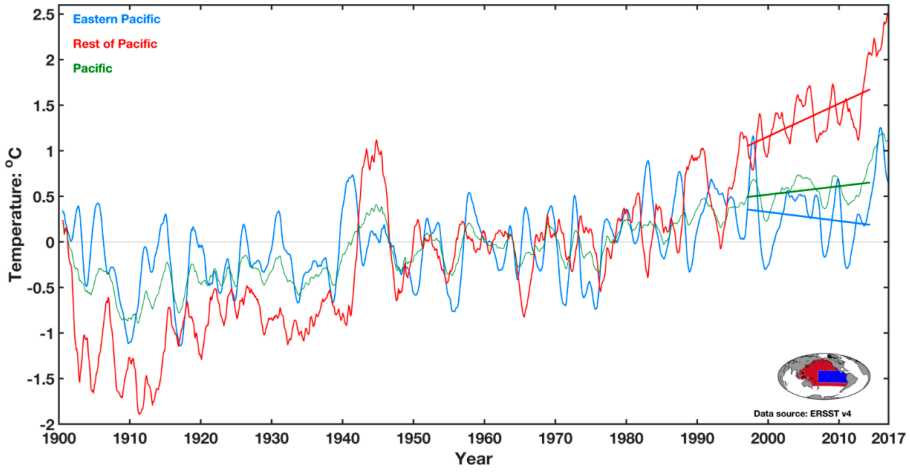

Figure 4. East vs. West Pacific SST (relative to 1961–1990 mean): The mean SST of the eastern tropical Pacific in blue curve (with weight = 1), and the mean SST of the rest of the Pacific (area weighted by 1.86). The mean SST for the Pacific basin as a whole is in green. The regions used are depicted in the inset. The blue region in the eastern Pacific is the same as that used in Kosaka and Xie [38] and is 35% of the Pacific basin. The SST time series have been smoothed using 27-month running mean. The linear trend, using the same color as the SST for each region, is objectively determined by least-square linear regression.

2.3. The Arctic

Cowtan and Way [52] raised a concern on the treatment of missing Arctic data (which should have a faster warming rate). On the other hand, Gleisner et al. [53] suggested that the high latitudes contributed only marginally. Uncertainties exist on the best ways to fill the gap, as discussed by Curry [54]. What Figure 3 shows is that the *observed* pace of global warming during this period has slowed markedly compared to previous two and half decade.

3. The Energy Budget

3.1. The Global Budget

When the global-mean surface temperature did not warm as expected in the presence of ever increasing atmospheric concentration of greenhouse gases, there can only be two possible reasons, both involving the energy budget of the earth: (1) the radiative heating was not appreciably reaching the surface—most of it presumably was reflected back to space by, for example, increasing aerosols from volcanic eruptions and anthropogenic pollution; or (2) that the heating was reaching the surface and below, but was sequestered in the oceans below the mixed layer. (Of course, a combination of the two is possible, for example, as in half from reduction of radiative forcing and half from ocean storage of heat.) It then follows that no resolution of the "mystery" of the global warming slowdown can be accomplished without a proper accounting of the "missing heat", including whether any heat was indeed "missing". The pioneering work of Meehl et al. [55,56] supports (2) as a possible explanation. They found in a coupled model that the surface hiatus periods are associated with enhanced storage of heat in the intermediate layers of the global oceans.

Let $\Delta H_{TOA} = H_{sw} - H_{lw}$ be the radiative imbalance between the short-wave (sw) and long-wave (lw) radiation at the top of the atmosphere (TOA) per unit area of the planet. Since the heat capacity of

the ocean is much larger than that of the atmosphere and of the cryosphere (93% since 1955, according to Levitus et al. [57]; see Trenberth et al. [58] for a review), we have, approximately

$$\Delta H_{TOA} = \frac{\delta}{\delta t} OHC_{total}, \quad (1)$$

where OHC_{total} is the total ocean heat content of the world's oceans. Loeb et al. [59] estimated that for the period 2001–2010, $\Delta H_{TOA} = 0.5 \pm 0.43$ W·m^{-2} using TOA satellite radiative measurements anchored to a well-observed but shorter period 2005–2010 of the ocean OHC change in 0–1800 m.

Using 0–1500 m OHC change as an approximation of the total OHC change since 2000, Chen and Tung [60] calculated, for the global ocean, a value for the right-hand side of Equation (1) as 0.49 W·m^{-2}, nearly matching the value given by Loeb et al. [59]. The observational uncertainty of subsurface data obtained by various instruments were reviewed by Abraham et al. [61]. After the launch of Argo floats since 2000 [62], the uncertainty has been much reduced. For the period in their review that overlaps with the current review, Levitus et al. [63] deemed the global data coverage to be nearly 100% at 700 m for $1 \times 1^{\circ}$ squares with at least 4 measurements in 5 years, including all instruments. Roemmich et al. [64] found the Argo data to be accurate and spatially homogenous after 2005. However, as pointed out by Cheng and Zhu [65], the rapid transition from non-Argo to Argo observing platform around 2002–2003 may have introduced an artifact in the Southern Ocean, where non-Argo observations were sparse. The data are here adjusted by us (shown in color in Figure 5, with the original unadjusted in grey) for the Southern Ocean to remove this artifact, following Cheng and Zhu. The adjustment does not affect data after 2003, but changes the slope of the OHC when referenced to year 2000. The 0–1500 m OHC of the global oceans is now seen to be increasing at the rate of ~0.42 W·m^{-2}, still close to the TOA net radiative imbalance, considering that the latter is more uncertain [59].

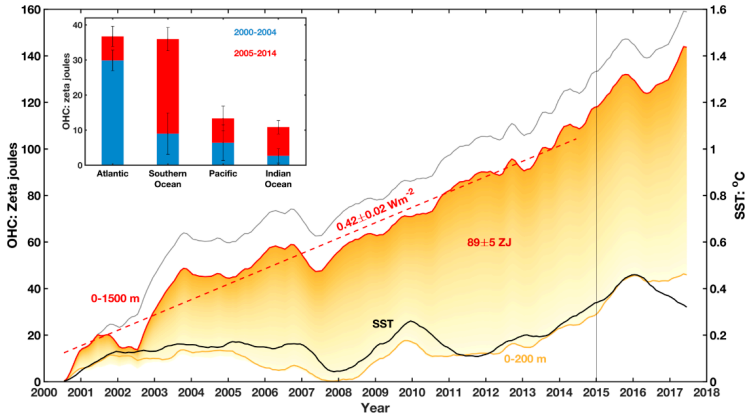

Figure 5. Global mean SST and OHC relative to 1998: SST from ERSST.v4 is in black and 0–200 m OHC in light orange curve, showing that they co-vary and both are in a warming slowdown, while the "total" OHC, as approximated by the 0–1500 m OHC in red curve, is increasing at the regressed linear rate of 0.42 W·m^{-2} (red dashed straight line). The orange shaded region is the amount of heat stored in the 200–1500 m layer, and it is about 89 zetajoules for the period 2000–2014. The data were adjusted by us for the Southern Ocean to remove a possible artifact due to the rapid transition from no-Argo to Argo observing platform around 2002–2003, as pointed out by Cheng and Zhu [65]. The original data [66] for the unadjusted 0–1500 m OHC are shown in grey. The inset shows the division of the 89 zetajoules of the global ocean increase in heat storage in 200–1500 m (linear trend multiplied by the number of years) into the four ocean basins. Note that the definition of the Southern Ocean in oceanography and here is south of 35S. The tip of the Drake Passage is at 38S. The error bars are from the linear trend regression. For the subsurface ocean heat content we use Ishii data [66], which is available up to 2012. Most of the recent measurements are from the Argo floats [62].

The question of why the SST is in a slowdown should also be asked of the upper 200 m of the global oceans; the two are highly correlated (r = 0.82) (Figure 5) and physically related. The mixed

layer varies in depth and with season in different parts of the oceans, but a rough global measure of its depth is about 200 m. Through wind and turbulence mixing, the temperature in the mixed layer is more uniform vertically and strongly influenced by surface processes. Given that the total OHC in a column is increasing, the reason that the upper 200 m OHC is not increasing must be due to the heat transported below 200 m. The difference between the 0–200 m and 0–1500 m OHC curves is the amount of heat stored between 200 m and 1500 m. This amount has increased from year 2000 to 2014 by approximately 89 $\pm$ 5 *zettajoules* (linear trend and regression error. 1 *zettajoule* = 10^{21} *joules*, about twice the world's energy consumption per year). When 89 *zettajoules* are divided by 15 years and the area of the planet, it yields 0.37 W·m^{-2} (1 W = 1 Js^{-1}). The small left-over 0.05 W·m^{-2} is why the upper 200 m of the global oceans warmed only slightly.

The ocean need not always behave this way. It could instead distribute the OHC mostly in the top 300 m, as it apparently did in the last two decades of the 20th century [60], when the surface warmed rapidly. Therefore this energy budget calculation argues in favor of the explanation that it is the oceans sequestering the heat below 200 m that would otherwise have warmed the surface, rather than a reduction of radiative forcing, as the major cause of the global warming slowdown. However, the latter explanation cannot be ruled out as a partial explanation, because the subsurface data were probably not good enough around the turn of the century for us to detect a small change in slope. Nevertheless, no large reduction of TOA radiative imbalance has been reported [67], and some datasets even reported an increase (see Trenberth et al. [58]).

3.2. Partition Among Different Ocean Basins

Of the 89 *zettajoules* of increased storage in the global oceans between 200 and 1500 m for 2000–2014, a majority of the heat storage increase (63 *zettajoules*, or 70%) occurred in the Atlantic and the Southern Oceans, with the Indian Ocean (14 *zettajoules*) and the Pacific (11 *zettajoules*) playing secondary roles (see Table 1). The Argo floats did not reach full coverage of the Southern Ocean until 2004 or 2005, but the coverage by a combination of expendable bathythermographs and Argo floats was probably adequate since 2000 in the North Atlantic. These instruments in the Atlantic showed that the Atlantic's uptake in the 200–1500 m layer was 31 *zettajoules* (60% of the corresponding global value) between 2000 and 2005, as AMOC sped up [68], thereby increasing the subduction of warm saline waters in the subpolar Atlantic [54]. AMOC then slowed after 2005, as measured by the RAPID array [69,70], and the Atlantic subducted little additional heat. Then the Southern Ocean picked up most of the heat storage, accounting for 27 *zetajoules* of heat in the layer between 200 m and 1500 m between 2005 and 2014 (54% of the global value). Thus, the Atlantic and the Southern Oceans in turn carried the majority of the increase in heat uptake in the 200–1500 m of the global ocean. This way of accounting does not use the poorer data of the Southern Ocean prior to 2005.

There are also some horizontal compensation of heat increase in the upper layers of the global ocean: Nieves et al. [71] commented on the cooling in the top 100 m of the eastern Pacific being compensated by warming in the 100–300 m layer of the Western Pacific and the Indian Ocean. Using a model simulation Lee et al. [47] suggested that the warming in the Indian Ocean has a Pacific origin: the intensified trade wind might have blown some of the warm water accumulated in the western Pacific over to the Indian Ocean through the Indonesian Through Flow. Since it is the only ocean basin that warmed appreciatively in the upper layer, Indian Ocean may account for a large *percentage* of the small global heat uptake in that layer (65% for the 0–200 m, see Table 1; 70% for 0–700 m, see Lee et al., and Chen and Tung [72]).

The dominance of the Southern Ocean in heat storage after 2005 was confirmed by Roemmich et al. [64], who examined the period 2006–2013, when Argo floats achieved global coverage. Nieves et al. [71] on the other hand found the Southern Ocean to be secondary to the Indian Ocean in heat storage increase since 2003 in terms of temperature trends. But, when multiplied by the smaller area of the Indian Ocean in the OHC calculation, the Indian Ocean should have become secondary to the Southern Ocean (see Table 1). Liu et al. [73] reexamined the observational analysis of Chen and

Tung [60]. In agreement with Chen and Tung [60], they found that "the Atlantic and the Southern Ocean contributed most to OHC increases at depths >300 m". For the layer 300–1500 m, they found that the percentage of the linear warming trend of the OHC in the Atlantic, Southern Ocean, Pacific and Indian Ocean to the global OHC warming trend during 1998–2012 are 33.8, 40.7, 8.2 and 15.8%, respectively, which were deemed similar to those during the longer period from 1970 to 2012—30.7, 41.3, 13.5 and 5.4%, respectively. Although they agreed with Chen and Tung [60] on the larger role played by the Atlantic and Southern Oceans, they argued that the larger heat uptakes in these ocean basins have not changed between the two periods and that fact should justify the interpretation that "the deep heat penetration in these two basins is not unique to the hiatus but is characteristic of anthropogenic warming". In a rebuttal, Chen and Tung [72] pointed to their misleading use of percentages instead of actual OHC magnitudes. The earlier, non-hiatus period, 1970–1997, was characterized by a small OHC increase of 12 zettajoules in the global oceans, while during the latter, hiatus period, 1998–2012, 58 zettajoules was sequestered in the 300–1500 m layer in the global oceans. The Atlantic's heat uptake into the 300–1500 m layer increased by a factor of over 4 during the hiatus period compared to the previous non-hiatus period, when measured in OHC magnitudes. Liu et al. [73]'s second conclusion, "that heat redistribution in the upper 350 m between the Pacific and Indian Oceans is closely tied to the surface warming hiatus", was also based on the larger percentage of heat storage increase in these two ocean basins in the upper layer. It can be seen in our Table 1 that it was a larger percentage of a very small magnitude of global OHC.

Table 1. Ocean Heat Content during different periods and in different ocean basins, expressed in zettajoules, obtained by multiplying the linear trend in each period by the number of years. (Unit: *zettajoule*).

	2000–2005	**2005–2014**	**2000–2014**
0–200 m			
Global	11 ± 6	21 ± 5	17 ± 4
Atlantic	14 ± 2	-7 ± 2	0 ± 2
Southern Ocean	-6 ± 3	11 ± 2	3 ± 2
Pacific	8 ± 4	4 ± 4	2 ± 3
Indian Ocean	-5 ± 1	13 ± 2	11 ± 1
200–1500 m			
Global	52 ± 7	50 ± 5	89 ± 5
Atlantic	31 ± 3	8 ± 3	26 ± 3
Southern Ocean	12 ± 6	27 ± 3	37 ± 3
Pacific	6 ± 5	7 ± 4	11 ± 3
Indian Ocean	3 ± 2	8 ± 2	14 ± 1

4. Proposed Mechanisms

A prerequisite for a decadal slowdown in *global-mean* warming must be a reduction of radiative heating available to the surface. This could come about from either a reduction of radiative forcing from above or from an enhanced uptake by the oceans below. In the first category, it has been proposed that a reduction of radiative forcing can arise by a decrease in stratospheric water vapor [74], an increase in background stratospheric volcanic aerosols [75], by 17 small volcano eruptions since 1999 [76], increasing coal-burning in China [77], the indirect effect of time-varying anthropogenic aerosols [28], or a low solar minimum [78]. These forcing reductions likely contributed no more than 20% of the slowdown [58]. Schmidt et al. [79] showed that a combination of a revised aerosol parameters applied to the recent moderate volcano eruptions and anthropogenic pollution from emergent China accounted for half of the discrepancy between CMIP5 models and observation, with the solar minimum and different phasing of ENSO one seventh. Asian pollution from coal burning however contain black carbon as well as sulphate aerosols, and Kühn et al. [80] found that the warming effect of the former offset the cooling due to the latter, yielding very little global or regional effect.

The 30-year mid-20th century hiatus was also thought to be caused by aerosols from pollution in an emergent economy after the war [28,81]. Because of the uncertainty associated with the aerosol

parameters and response, it is difficult to assess the efficacy of the proposals. However, aerosol cooling of the surface of the ocean from above should destabilize the ocean's vertical stratification, and there should be a subsurface signature but none was found. Zhang et al. [29] pointed out that the subsurface observations in the Atlantic showed warming, in contrast to the modeled subsurface aerosol cooling. Chen and Tung [60] found subsurface signature of salinity and heat content variations during the mid-20th century hiatus to be that of an internal ocean variability of increased heat uptake, similar to the current one.

Kosaka and Xie [38] focused on the cold eastern equatorial Pacific as the main driver for the global warming slowdown. Their results demonstrated dramatically that the slowdown in global warming could be simulated when the observed SST in this cold-tongue region is specified in a climate model that does not by itself produce the slowdown. What caused the eastern Pacific to have more of the cold La Niña-type than the warm El Niño-type of events in observation—but not in the original model—was not pursued. While it is well known that the interannual part of ENSO influences the interannual variation of the global-mean surface temperature through atmospheric teleconnections [82,83], the influence of the multidecadal variability in the Pacific on the global mean is much more subtle, as will be discussed in Section 5 on model "nudging" experiments. England et al. [39] proposed that the intensification of the trade wind in the tropical Pacific is the cause for the global warming hiatus, by creating the La Niña-type pattern in the eastern Pacific SST. They attributed this observed 20-year intensification of the Pacific trade winds to the negative phase of the Interdecadal Pacific Oscillation (IPO) [84], though the coauthors later casted doubt on that assertion [39]. Dai et al. [85] concluded that internal climate variability, "mainly through IPO, was largely responsible for the recent slowdown". In a *Perspective* in *Science*, Clement and DiNezio [86] gave a short review of the literature up to that time, arriving at a tentative conclusion that the Pacific is the "driver" of the observed decadal change in the current period, and much of the evidence in the papers reviewed rested ultimately on the IPO and its kin, Pacific Decadal Oscillation [87] (PDO).

Meehl and Hu [88] gave the only mechanistic explanation of the IPO as wind-stress forced Rossby waves at 20N and 25S crossing the Pacific, with a decadal transit time, setting the timescale of the portion of the IPO spectrum in the 20–30 year period, but not the 60–70 year period now alluded to as explaining the multidecadal variability in the global-mean temperature seen in Figure 2. We will discuss the IPO later in Section 6 and address whether or not it is "ENSO-like".

Intensifying trade wind is not expected to subduct appreciable heat in the tropical Pacific, or for that matter, in the Pacific as a whole (see Figures 3 and 5 inset). Huang [89] investigated the adjustment of OHC in response to the wind-driven circulation in the form of "heaving" of the isopycnal surfaces and suggested that the adiabatic movement of warm water along such sloping surfaces as a mechanism for vertical redistribution of heat in the oceans. However, he concluded: "heat content variability inferred from our model is at least one order of magnitude smaller than the mean warming rate inferred from observations".

In the Atlantic, the multidecadal variability in the SST is understood from modeling studies to be caused by the variations of subsurface AMOC. "Water hosing" experiments of Zhang et al. [25] suggest that freshening of subpolar North Atlantic waters can lead to a slowdown of AMOC and a cooling of the surface temperature under preindustrial conditions. In the presence of top-of-atmosphere radiative imbalance, Chen and Tung [60] showed using subsurface ocean data, including salinity and ocean heat content, that as the AMOC sped up during 1999–2005, it subducts heat in the subpolar latitudes of the North Atlantic. That this is a period of increasing overturning in the Atlantic was previously calculated by Willis [68] using satellite altimetry data available since 1993. The proposed mechanism is as follows: As AMOC speeds up, it brings the warmer and more saline subtropical surface water to the sub-polar latitudes of the Atlantic, where it loses part of its heat to the cold atmosphere and sinks due to its saltiness. The heat released by the warm water to the atmosphere melts glacier ice over Greenland and the surrounding areas bounding the North Atlantic, gradually leading to a freshening of the North Atlantic water that eventually slows the sinking. As AMOC slows, its northward transport of heat slows and the freshwater outflow from glacier ice melt is reduced. Salinity and hence density of the

seawater build up slowly over decades, until it is dense enough to initiate another speeding up of the AMOC. In this way the AMOC alternately speeds up and slows, taking approximately 60–70-years for a full cycle, leading to warmer and colder AMO at the sea surface with the same multi-decadal variations. A more detailed discussion can be found in Sarachik et al. [90]. Most recent CMIP5 models tend to have 20–30-year oscillations [91], with the exception of MPI and an older version of GFDL model.

Figure 6 compactly shows the OHC changes in the four ocean basins. The size of the different ocean basins is taken into account. Figure 6a,b show that before 2005, the North Atlantic subducted a large amount of heat through deep convection down to at least 1500 m in the subpolar Atlantic, caused by a sped-up AMOC [60]. After 2005, AMOC slowed and the deep convection reduced. There is cooling in the subpolar Atlantic, but warming in the subtropical Atlantic due to the northward displacement of the Gulf Stream as AMOC slowed [92]. Figure 6c,d are meridional integral of the Pacific and Indian Oceans as a function of longitude. There was a continuous trend of trade wind intensification over both periods, creating a La Niña mean state in the eastern tropical Pacific. The intensifying trade wind blows more warm surface water from the eastern Pacific to the western Pacific, and a little over the Indonesian Through Flow into the upper layer of the Indian Ocean, which can be seen clearly in this figure. Its magnitude of warming is relatively small and it is shallow and located near the Indonesian Through Flow opening to the Pacific. This figure adds observational confirmation of the possible Pacific origin of the Indian Ocean warming [47]. Indian Ocean's shallow warming is a secondary player in the heat sequestration in the energy budget below 200 m, consistent with Figure 5 and Table 1. In the Pacific, the heat sequestered in the western Pacific is large, but the change is mostly balanced by the cooling in the eastern Pacific above 300 m in the two periods. When summed over the basin, Pacific also plays a minor role in the energy budget, as shown in Figure 5 and Table 1. In the Southern Ocean, the heat storage increase is large after 2005 when integrated over the circumpolar band of the ocean. The larger magnitude is due to the larger area being integrated over in the circumpolar band in our way of accounting for the total contribution to the global OHC. Locally the warming is not particularly intense in the Southern Oceans. The increase appears to be a continuation of the warming from 1990s, but the data before 2004 was not adequate.

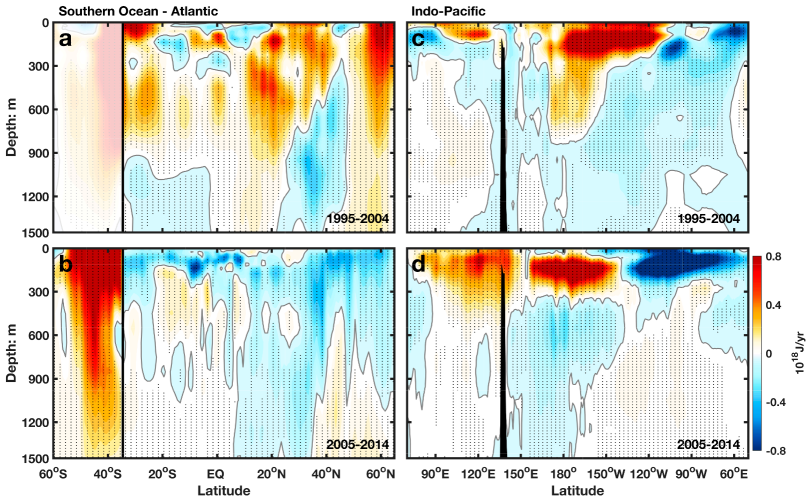

Figure 6. Linear trend of OHC cross-sections: (**a**,**b**) linear trends in the two periods indicated, zonally integrated (not averaged) over the longitude of the Atlantic basin as a function of latitude. South of 35S, the zonal integration is circumpolar (skipping over the land). The thin black line at 35S separates the two latitude regions with very different zonal extents. (**c**,**d**) OHC linear trends in the two periods indicated, as a function of longitude in the Indo-Pacific sector, meridionally integrated (not averaged) from 35S to the northern boundary of the ocean basins. The topography in the Indonesia Through Flow is 8S–8N averaged and shown in black. Top two panels are linear trends over 1995–2004. Bottom two panels are the linear trends over 2005–2014. Each period is 10 years. The Southern Ocean part is blanked out in (**a**) due to poor data quality. Regions where signal is statistically significant above 95% confidence level are stippled.

5. Model "Nudging" Results and Their Interpretations

The unexpected slowdown in global warming offers lessons that can help future climate model developments. Fyfe and Gillett [51] noted the severe discrepancy that existed in the eastern Pacific, with the observed SST much colder than any of the model runs. Kosaka and Xie [38] attempted to remedy this deficiency in the GFDL model by specifying from observation the colder eastern equatorial Pacific SST. The model surface air temperature (SAT) over this region was initially warmer than observed. Model "SST is restored to the observed evolution by a Newtonian cooling over the deep tropical eastern Pacific". Thus a numerical heat sink was introduced, absorbing whatever energy is needed to bring the model SST in that region back to the observed cold temperature. The atmosphere always tends to move heat from other (warmer) regions into the cold eastern Pacific to be absorbed, eventually yielding a global hiatus with just enough heat transported to this region to be absorbed, and the model SAT becomes compatible with the specified observed SST, meaning that the model SAT becomes close to the observed SAT. One may be able to assess whether the Pacific heat sink in the model is consistent with the observed OHC in the Pacific to provide a crucial check on the reasonableness of the proposed mechanism. However, the model diagnosed heat flux in the ocean was "overridden" in the nudging experiment of Kosaka and Xie [38], and so the amount of heat uptake cannot be compared with observation. But such information is available in another model (see later).

This effect on heat absorption in the eastern Pacific is not as prominent in a model setup where the observed atmospheric field is specified, as in Drijfhout et al. [93], because the SAT over the cold SST is also cold. Instead of specifying the wind field only in the tropical Pacific, Drijfhout et al. [93] specified the meteorological field throughout the globe, and found that it drove an increase in ocean heat uptake of 0.5 $W \cdot m^{-2}$ during 2001–2009 over 1992–2000. The Southern Ocean (south of 35S) and the subpolar North Atlantic were dominantly responsible for such an increase, and the tropical Pacific less so. Watanabe et al. [94] specified the wind stress from observation for 30S–30N over the world oceans, including the tropical Atlantic, not just over the Pacific. Zonal mean subsurface temperature of the world oceans, which was allowed to adjust, was shown by Watanabe et al. [94] and compared favorably with observation, pointing to the importance of high latitude oceans, especially the North Atlantic, in deep heat sequestration. The high-latitude response in the model is remotely forced by the nudged tropical Atlantic winds, and is absent in the experiment of England et al. [39], where only the Pacific winds are nudged. Inferred regions of heat sink from "nudging" experiments are seen to be sensitive to the region of "nudging". Douville et al. [95] suggested that the nudging or pacemaker experiment should include not just the tropical Pacific but also the North Atlantic. In addition Douville et al. [95] found that most climate models underestimate the potential role of North Atlantic ocean while overestimate the influence of ENSO on global-mean surface temperature (GMST). In particular "none of the CMIP5 models is able to capture the observed persistent positive correlations between AMV and GMST, which might explain why the role of North Atlantic multi-decadal variability has been so far much less tested than the role of the tropical Pacific."

Trenberth et al. [96] showed that a somewhat better simulation is obtained over Eurasia if the negative latent heating implied by the cold (and dry) eastern and central Pacific SST is put aloft instead of at the surface, using an atmosphere-only model.

Meehl et al. [55,56] were the first to show in a coupled model without nudging that periods of global-warming hiatus occur even though the model top-of-the atmosphere radiative imbalance happens to be constant. They attributed the internal ocean variability to the IPO, the AMOC and the Antarctic Bottom Water. Guemas et al. [97] in a retrospective prediction of the surface hiatus of the past decade attributed the onset to an increase in ocean heat uptake in the Pacific and Atlantic. Meehl et al. [98] suggested that if model's IPO is made to coincide with observation, CMIP5 models could possibly predict the slowdown.

6. IPO as an Interdecadal Modulation of ENSO

The IPO came to the public's attention recently as the role of internal multidecadal climate variability in influencing the global surface temperature is increasingly recognized in the scientific

literature. Two appealing aspects of the IPO/PDO have often been alluded to: (i) the phase of the IPO appears to coincide with the "climate regime shifts" in the global-mean surface temperature, so that by implication the former causes the latter, and (ii) its spatial pattern is "ENSO-like" and therefore it implicates the tropical Pacific [39,84,96]. It turns out that neither of these attributes is robust.

As a low-frequency modulation of ENSO, IPO is obtained by performing Empirical Orthogonal Function (EOF) decomposition on the low-passed SST data using a Fourier filter. A reasonable 15-year low passed filter, reasonable for getting the "interdecadal oscillation", is sufficient in filtering out the high variance, high-frequency ENSO in the tropical Pacific, leaving very little ENSO-related signature. This is consistent with the historical definition of IPO by Folland et al. [84]. A 13.3-year low-pass filter was used to "remove ENSO-related variability". As a consequence, their IPO does not have the ENSO-related variability in the eastern tropical Pacific. They used 84 years of SST data, from 1911–1995. The degrees of freedom is extremely small after low passed by a 13.3 year filter [99]. Later Parker et al. [100] extended the record backward by 20 year to 1891, used an 11-year low-pass filter and redefined the second EOF of the low-pass global SST as the IPO. Its spatial pattern has what appears to be a more prominent ENSO-related variability in the tropical eastern Pacific. Tung et al. [101] reexamined Parker et al.'s calculation, removing the poorer quality data prior to 1911. The "ENSO-related" feature of Parker et al.'s IPO largely disappears, and remains absent when 20 more years of recent data are added to the end of the time series. Because of the closeness of the eigenvalues in the EOF analysis of decadally filtered SST, the second and third EOFs form what North et al. [102] called "effectively degenerate multiplet" within the large sampling error of the finite sample. Some authors used the second EOF as the IPO and others chose the third EOF. The second EOF looks more like the AMO while the third more like the PDO. They are in effect not distinct because of the degeneracy.

Despite its name, the main component of the IPO is actually the AMO, along with some PDO and ENSO. They are "mode-mixed" because of the low-pass filtering. See Figure 7, showing the composition of the IPO. At decadal filtering commonly used, ENSO is almost entirely filtered out. There is a small trend (TR) and a small PDO component. The largest component is the AMO. Chen and Tung [7] found that it is actually the AMO component in some of the IPO indices that appear to mimic the low frequency variation of the global-mean surface temperature. The PDO contributes very little to the global-mean surface temperature (see Figure 8), because of its compensating warm and cold centers of action, as shown in more detail in Chen and Tung [7].

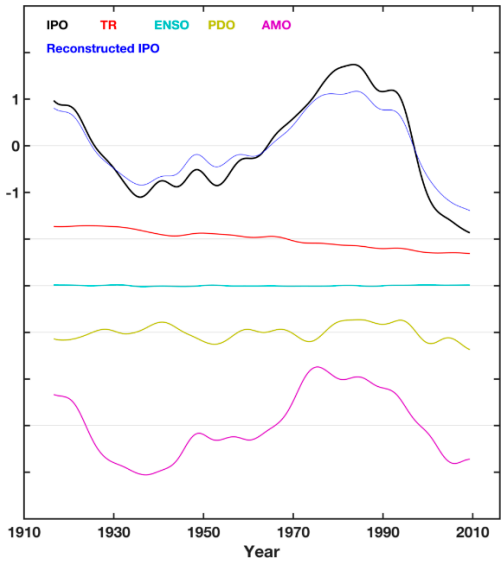

Figure 7. The composition of the IPO. IPO index in black. The composition of the IPO as reconstructed using the sum of its four leading components in blue. The individual component is also shown. It is dominated by the AMO. IPO is here defined as the second Principle Component of 13-year low-pass filtered SST. Reproduced from Chen and Tung [7].

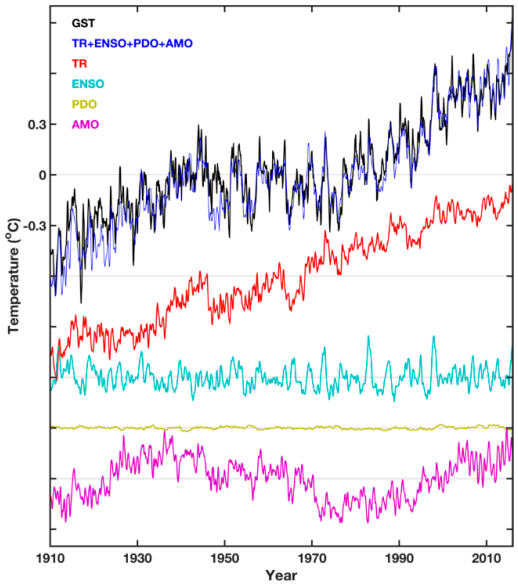

Figure 8. The global-mean surface temperature (GST). Shown are the four orthogonal components of the GST of unfiltered data as a function of time. Each curve has been offset vertically by 0.2. From top to bottom, GST and the sum of the first 4 components. They are the trend mode (TR), the ENSO-cycle mode (ENSO), the global PDO mode (PDO), and the global AMO mode. Reproduced from Chen and Tung [7].

7. Conclusions

Although IPCC referred to the 15-year period 1998–2012 as the "hiatus", the trend to 2014 as reported by Karl et al. [2] disqualifies the period to 2014 as a "hiatus", but it can still be considered a "slowdown". The appearance of the "warm blob" in the north Pacific [103,104], possibly due to air-sea interaction, made 2014 a warm year, but that phenomenon did not last. Then came the extreme El Nino of 2015–2016, producing record surface temperature globally. So the period of slowdown probably ended in 2014.

In trying to understand this phenomenon the community, through intensive modeling and analysis efforts, seemed to have gained a better recognition of the role of multidecal internal variability in climate change and a clearer assessment of various factors of external forcing. The new Argo data allowed a glimpse of the global oceans below the surface about the possible pathways of heat uptake.

Multidecadal variations in the global surface temperature were previously noted [20,33,34,105], and the negative phase of the recent cycle appears to account for the slowdown in warming in the 21st century. The spatial pattern of this variability contributing to the global mean was found to center in the North Atlantic, and much weaker in the Pacific [20] (Figure 3). There was indeed a cooling trend in the eastern tropical Pacific for 1997–2014, but there was a compensating warming trend in the western Pacific (Figure 4), explainable by the trade wind blowing warm surface water from the east to the west Pacific.

Although many in the scientific literature attribute the current (and prior) episode of the warming slowdown to the IPO, significant mathematical issues exist with its definition [101] due to its extremely low degrees of freedom. The ENSO-related spatial pattern often referred to as the IPO was found to be an artifact of strong sensitivity to sparse data prior to 1910. When that part of the data was excluded, the spatial pattern is no longer ENSO-like, along with the implication that IPO modulates ENSO. This was shown in Tung et al. [101]. The time series of the IPO which appears to coincide with the multidecadal variation of the global-mean surface temperature turns out to be the AMO component contained in the IPO. Low-pass filtering of the SST in the definition of IPO mixes AMO with PDO.

"Nudging" experiments focused on the Pacific produced a slowdown in warming probably because of the presence of a numerical sink of heat introduced. That the numerical sink was introduced

in the Pacific in these numerical experiments probably should not be interpreted as where the real sink should be located. When wind stress was specified over pan tropical oceans instead of just over the eastern tropical Pacific, large deep heat sequestration is found in high latitude oceans, especially the North Atlantic, instead of over the equatorial ocean. It is now known that "nudging" or "pacemaker" experiments are sensitive to experimental setup, and it was suggested that surface conditions in other ocean basins, including the tropical Atlantic, should be included.

In a somewhat related study on the transient climate sensitivity of CMIP5 coupled climate models to 4 × CO_2 forcing, Kostov et al. [106] found that "a substantial portion of the global ocean heat uptake occurs within a relative small region in the North Atlantic and that anomalous heat is advected to depth along the upper AMOC cell" and intermodal differences in response to the greenhouse forcing "can be understood in terms of variations in the depth of heat storage, which in turn reflects the depth and strength of the AMOC." "Models with a deeper and stronger overturning circulation store more heat at intermediate depths, which delays the surface temperature response on multidecadal time scales". This model result is consistent with the observational evidence presented here.

Observed subsurface ocean heat content data show that the major sinks of heat are in the North Atlantic and the Southern Ocean, accounting for a majority of the heat stored in the intermediate layers of the world's oceans, although the debate continues regarding whether it is the Pacific-Indian oceans on one side or Atlantic-Southern Oceans on the other side that is mostly responsible for causing the warming slowdown. Regardless, the result so far favors the explanation of the warming slowdown as an internal variability of the ocean's ability in storing the heat that otherwise would have warmed the surface more.

Author Contributions: K.-K.T. and X.C. conceived and designed the experiments; X.C. analyzed the data and contributed analysis tools; K.-K.T. led the writing of the paper.

Funding: The research of K.-K.T. was funded by National Science Foundation, under AGS-1262231 and Frederic and Julia Wan Endowed Professorship. X.C. was funded by the National Key Basic Research Program of China under Grant 2015CB953900, the Natural Science Foundation of China, under 41776032, and Natural Science Foundation of China- Shandong Joint Fund for Marine Science Research Centers under Grant U1606402.

Conflicts of Interest: The authors declare no conflict of interest.

References

1. Stocker, T.F.; Qin, D.; Plattner, G.-K.; Tignor, M.; Allen, S.K.; Boschung, J.; Nauels, A.; Xia, Y.; Bex, V.; Midgley, P.M. *IPCC, Climate Change 2013: The Physical Science Basis. Contribution of Working Group I 2013*; Cambridge University Press: Cambridge, UK; New York, NY, USA, 2013.
2. Karl, T.R.; Arguez, A.; Huang, B.; Lawrimore, J.H.; McMahon, J.R.; Menne, M.J.; Peterson, T.C.; Vose, R.S.; Zhang, H.-M. Possible artifacts of data biases in the recent global surface warming hiatus. *Science* **2015**, *348*, 1469–1472. [CrossRef] [PubMed]
3. Yan, X.-H.; Boyer, T.; Trenberth, K.; Karl, T.R.; Xie, S.-P.; Nieves, V.; Tung, K.-K.; Roemmich, D. The global warming hiatus: Slowdown or redistribution? *Earths Future* **2016**, *4*, 472–482. [CrossRef]
4. Morice, C.P.; Kennedy, J.J.; Rayner, N.A.; Jones, P.D. Quantifying uncertainties in global and regional temperature change using an ensemble of observational estimates: The HadCRUT4 data set. *J. Geophys. Res.* **2012**, *117*. [CrossRef]
5. GISS Surface Temperature Analysis (GISTEMP). NASA Goddard Institute for Space Studies. 2018. Available online: https://data.giss.nasa.gov/gistemp/ (accessed on 1 October 2018).
6. Dee, D.P.; Uppala, S.M.; Simmons, A.J.; Berrisford, P.; Poli, P.; Kobayashi, S.; Andrae, U.; Balmaseda, M.A.; Balsamo, G.; Bauer, P.; et al. The ERA-Interim reanalysis: Configuration and performance of the data assimilation system. *Q. J. R. Meteorol. Soc.* **2011**, *137*, 553–597. [CrossRef]
7. Chen, X.; Tung, K.K. Global mean surface temperature variability—Space-time perspective from rotated EOFs. *Clim. Dyn.* **2017**. [CrossRef]
8. Zhang, R. On the persistence and coherence of subpolar sea surface temeprature and salinity anomalies associated with the Atlantic multidecadal variability. *Geophy. Res. Lett.* **2017**, *44*, 7865–7875. [CrossRef]

9. Zhang, R.; Delworth, T.L.; Held, I.M. Can the Atlantic Ocean drive the observed multidecadal variability in Northern Hemisphere mean temperature? *Geophy. Res. Lett.* **2007**, *34*. [CrossRef]
10. Zhang, R. Coherent surface-subsurface fingerprint of the Atlantic meridional overturning circulation. *Geophys. Res. Lett.* **2008**, *35*. [CrossRef]
11. Delworth, T.L.; Mann, M.E. Observed and simulated multidecadal variability in the Northern Hemisphere. *Clim. Dyn.* **2000**, *16*, 661–676. [CrossRef]
12. Chen, X.; Tung, K.K. Global surface warming enhanced by weak Atlantic Overturning Circulation. *Nature* **2018**, *559*, 387–391. [CrossRef] [PubMed]
13. Solomon, S.; Qin, D.; Manning, M.; Chen, Z.; Marquis, M.; Averyt, K.B.; Tignor, M.; Miller, H.H. *Climate Change 2007, Working Group I: The Physical Science Basis*; Cambridge University Press: Cambridge, UK; New York, NY, USA, 2007.
14. Thompson, D.W.J.; Solomon, S. Interpretation of recent Southern Hemisphere climate change. *Science* **2002**, *296*, 895–899. [CrossRef] [PubMed]
15. Brohan, P.; Kennedy, J.J.; Harris, I.; Trett, S.F.B.; Jones, P.D. Uncertainty estimates in regional and global observed temperature changes: A new data set from 1850. *J. Geophys. Res.* **2006**, *111*. [CrossRef]
16. Zhang, Y.; Wallace, J.M.; Battisti, D.S. ENSO-like interdecadal variability: 1900–1993. *J. Clim.* **1997**, *10*, 1004–1020. [CrossRef]
17. Chen, X.; Wallace, J.M. ENSO-like variability 1900–2013. *J. Clim.* **2015**, *28*, 9623–9641. [CrossRef]
18. Drijfhout, S.; van Oldenborgh, G.J.; Cimatoribus, A. Is a decline of AMOC causing the warming hole above the North Atlantic in observed and modeled warming patterns. *J. Clim.* **2012**, *25*, 8373–8379. [CrossRef]
19. Wu, Z.; Huang, N.E. Ensemble empirical mode decomposition: A noise-assisted data analysis method. *Adv. Adapt. Data Anal.* **2009**, *1*, 1–14. [CrossRef]
20. Wu, Z.; Huang, N.E.; Wallace, J.M.; Smoliak, B.; Chen, X. On the time-varying trend in global-mean surface temperature. *Clim. Dyn.* **2011**, *37*, 759–773. [CrossRef]
21. Folland, C.K.; Palmer, T.N.; Parker, D.E. Sahel rainfall and worldwide sea temperatures. *Nature* **1986**, *320*, 602–606. [CrossRef]
22. Knight, J.R.; Allan, R.J.; Folland, C.K.; Vellinga, M. A signature of persistent natural thermohaline circulation cycles in observed climate. *Geophys. Res. Lett.* **2005**, *32*. [CrossRef]
23. Schlesinger, M.E.; Ramankutty, N. An oscillation in the global climate system of period 65–70 years. *Nature* **1994**, *367*, 723–726. [CrossRef]
24. Schlesinger, B.M.; Ramankutty, N.; Andronova, N. Temperature oscillations in the North Atlantic. *Science* **2000**, *28*, 547–548. [CrossRef] [PubMed]
25. Zhang, R.; Delworth, T.L. Simulated Tropical Response to a Substantial Weakening of the Atlantic Thermohaline Circulation. *J. Clim.* **2005**, *18*, 1853–1860. [CrossRef]
26. Clement, A.; DiNezio, P.; Deser, C. Rethinking the ocean's role in the Southern Oscillation. *J. Clim.* **2011**, *24*, 4056–4072. [CrossRef]
27. Newman, M.; Compo, G.P.; Alexander, M.A. ENSO-forced variability of the Pacific decadal oscillation. *J. Clim.* **2003**, *16*, 3853–3857. [CrossRef]
28. Booth, B.B.B.; Dunstone, N.J.; Halloran, P.R.; Andrews, T.; Bellouin, N. Aerosols implicated as a prime dirver of twentieth-century North Atlantic climate variability. *Nature* **2012**, *484*, 228–232. [CrossRef] [PubMed]
29. Zhang, R.; Delworth, T.L.; Sutton, R.; Hodson, D.L.; Dixon, K.W.; Held, I.M.; Kushnir, Y.; Marshalln, J.; Ming, Y.; Msadek, R.; et al. Have aerosols caused the observed Atlantic Multidecadal Variability? *J. Atmos. Sci.* **2013**, *70*, 1135–1144. [CrossRef]
30. Gray, S.T.; Graumlich, L.J.; Betancourt, J.L.; Pederson, G. A tree-ring based reconstruction of the Atlantic Multidecadal Oscillation since 1567 A.D. *Geophys. Res. Lett.* **2004**, *31*. [CrossRef]
31. Chylek, P.; Folland, C.K.; Frankcombe, L.; Dijkstra, H.A.; Lesins, G.; Dubey, M.K. Greenland ice-core evidence for spatial and temporay variability of the Atlantic Multidecadal Oscillation. *Geophys. Res. Lett.* **2012**, *39*. [CrossRef]
32. Chylek, P.; Folland, C.K.; Lesins, G.; Dubey, M.K. Twentieth century bipolar seesaw of the Arctic and Antarctic surface air temperatures. *Geophys. Res. Lett.* **2010**, *37*. [CrossRef]
33. Tung, K.K.; Zhou, J. Using data to attribute episodes of warming and cooling in instrumental records. *Proc. Natl. Acad. Sci. USA* **2013**, *110*, 2058–2063. [CrossRef] [PubMed]

34. DelSole, T.; Tippett, M.K.; Shukla, J. A significant component of unforced multidecadal variability in the recent acceleration of global warming. *J. Clim.* **2011**, *24*, 909–926. [CrossRef]
35. Wei, W.; Lohmann, G. Simulated Atlantic Multidecadal Oscillation during the Holocene. *J. Clim.* **2012**. [CrossRef]
36. Yang, X.; Rosati, A.; Zhang, S.; Delworth, T.L.; Gudgel, R.G.; Zhang, R.; Vecchi, G.; Anderson, W.; Chang, Y.S.; DelSole, T.; et al. A Predictable AMO-Like Pattern in the GFDL Fully Coupled Ensemble Initialization and Decadal Forecasting System. *J. Clim.* **2013**, *26*, 650–661. [CrossRef]
37. Mahajan, S.; Zhang, R.; Delworth, T. Impact of the Atlantic Meridional Overturning Circulation (AMOC) on Arctic surface air temperature and sea ice variability. *J. Clim.* **2011**, *24*, 6573–6581. [CrossRef]
38. Kosaka, Y.; Xie, S.-P. Recent global-warming hiatus tied to equatorial Pacific surface cooling. *Nature* **2013**, *501*, 403–407. [CrossRef] [PubMed]
39. England, M.H.; McGregor, S.; Spence, P.; Meehl, G.A.; Timmermann, A.; Cai, W.; Gupta, A.S.; McPhaden, M.J.; Purich, A.; Santoso, A. Recent intensification of wind-driven circulation in the Pacific and the ongoing warming hiatus. *Nat. Clim. Chang.* **2014**, *4*, 222–227. [CrossRef]
40. Han, W.; Meehl, G.A.; Hu, A.; Alexander, M.A.; Yamagata, T.; Yuan, D.; Ishii, M.; Pegion, P.; Zheng, J.; Hamlington, B.D.; et al. Intensification of decadal and multi-decadal sea level variability in the western tropical Pacific during recent decades. *Clim. Dyn.* **2014**, *43*, 1357–1379. [CrossRef]
41. Delworth, T.L.; Zeng, F.; Rosati, A.J.; Vecchi, G.A.; Wittenberg, A.T. A link between the hiatus in global warming and North American drought. *J. Clim.* **2015**, *28*, 3834–3845. [CrossRef]
42. Merrifield, M. A shift in western tropical Pacific sea level trends during the 1990s. *J. Clim.* **2011**, *24*, 4126–4138. [CrossRef]
43. Timmermann, A.; McGregor, S.; Jin, F.-F. Wind effects on past and future regional sea level trends in the southern Indo-Pacific. *J. Clim.* **2010**, *23*, 4429–4437. [CrossRef]
44. Luo, J.J.; Sasaki, W.; Masumoto, Y. Indian Ocean warming modulates Pacific climate change. *Proc. Natl. Acad. Sci. USA* **2012**, *109*, 18701–18706. [CrossRef] [PubMed]
45. McGregor, S.; Timmermann, A.; Stuecker, M.F.; England, M.H.; Merrifield, M.; Jin, F.-F.; Chikamoto, Y. Recent Walker circulation strengthening and Pacific cooling amplified by Atlantic warming. *Nat. Clim. Chang.* **2014**, *4*, 888–892. [CrossRef]
46. Li, X.; Xie, S.-P.; Gille, S.T.; Yoo, C. Atlantic-induced pan-tropical climate change over the past three decades. *Nat. Clim. Chang.* **2016**, *6*, 275–279. [CrossRef]
47. Lee, S.-K.; Park, W.; Baringer, M.O.; Gordon, A.L.; Huber, B.; Liu, Y. Pacific origin of the abrupt increase in Indian Ocean heat content during the warming hiatus. *Nat. Geosci.* **2015**, *8*, 445–449. [CrossRef]
48. Clement, A.C.; Seager, R.; Cane, M.A.; Zebiac, S.E. An ocean dynamical thermostat. *J. Clim.* **1996**, *9*, 2190–2196. [CrossRef]
49. Tung, K.K.; Zhou, J. The Pacific's Response to Surface Heating in 130 Years of SST: La Nina-like or El Nino-like? *J. Atmos. Sci.* **2010**, *67*, 2649–2657. [CrossRef]
50. Kohyama, T.; Hartmann, D.L.; Battisti, D.S. La Nina-like mean state response to global warming and potential oceanic roles. *J. Clim.* **2017**, *30*, 4208–4225. [CrossRef]
51. Fyfe, J.; Gillett, N.P. Recent observed and simulated warming. *Nat. Clim. Chang.* **2014**, *4*, 150–151. [CrossRef]
52. Cowtan, K.; Way, R.G. Coverage bias in the HadCRUT4 temperature series and its impact on recent temperature trends. *Q. J. R. Meteorol. Soc.* **2014**, *140*, 1935–1944. [CrossRef]
53. Gleisner, H.; Thejll, P.; Christiansen, B.; Nielsen, J.K. Recent global warming hiatus dominated by low-latitude temperature trends in surface and troposphere data. *Geophys. Res. Lett.* **2015**, *42*, 510–517. [CrossRef]
54. Curry, J. Climate science: Uncertain temperature trend. *Nat. Geosci.* **2014**, *7*, 83–84. [CrossRef]
55. Meehl, G.A.; Hu, A.; Arblaster, J.M.; Fasullo, J.T.; Trenberth, K. Externally forced and internally generated decadal climate variability associated with the Interdecadal Pacific Oscillation. *J. Clim.* **2013**, *26*, 7298–7310. [CrossRef]
56. Meehl, G.A.; Arblaster, J.M.; Fasullo, J.T.; Hu, A.; Trenberth, K. Model-based evidence of deep-ocean heat uptake during surface-temperature hiatus periods. *Nat. Clim. Chang.* **2011**, *1*, 360–364. [CrossRef]
57. Levitus, S.; Antonov, I.; Boyer, T.P.; Locarnini, R.A.; Garcia, H.E.; Mishonov, A. Global ocean heat content 1955-2008 in light of recently revealed instrumentation problems. *Geophys. Res. Lett.* **2009**, *36*. [CrossRef]
58. Trenberth, K.E.; Fasullo, J.T.; Balmaseda, M.A. Earth's energy imbalance. *J. Clim.* **2014**, *27*, 3129–3144. [CrossRef]
59. Loeb, N.G.; Lyman, J.M.; Johnson, G.C.; Allan, R.P.; Doelling, D.R.; Wong, T.; Soden, B.J.; Stephens, G.L. Observed changes in top-of-the-atmosphere radiation and upper-ocean heating consistent within uncertainty. *Nat. Geosci.* **2012**, *5*, 110–113. [CrossRef]

60. Chen, X.; Tung, K.K. Varying planetary heat sink led to global-warming slowdown and acceleration. *Science* **2014**, *345*, 897–903. [CrossRef] [PubMed]
61. Abraham, J.P.; Baringer, M.; Bindoff, N.L.; Boyer, T.; Cheng, L.J.; Church, J.A.; Conroy, J.L.; Domingues, C.M.; Fasullo, J.T.; Gilson, J.; et al. A review of global mean temperature observations: Implications for ocean heat content estimates and climate change. *Rev. Geophys.* **2013**, *51*, 450–483. [CrossRef]
62. Roemmich, D.; Argo-Steering-Team. Argo: The challenge of continuing 10 years of progress. *Oceanography* **2009**, *22*, 46–55. [CrossRef]
63. Levitus, S.; Antonov, I.; Boyer, T.P.; Baranova, O.K.; Garcia, H.E.; Locarnini, R.A.; Mishonov, A.; Reagan, J.R.; Seidov, D.; Yarosh, E.S.; et al. World ocean heat content and thermosteric sea level change (0–2000 m), 1955–2010. *Geophys. Res. Lett.* **2012**, *39*. [CrossRef]
64. Roemmich, D.; Church, J.; Gilson, J.; Monselesan, D.; Sutton, P.; Wijffels, S. Unabated planetary warming and its ocean structure since 2006. *Nat. Clim. Chang.* **2015**, *5*, 240–245. [CrossRef]
65. Cheng, L.J.; Zhu, J. Artifacts in variations of ocean heat content induced by the observation system changes. *Geophys. Res. Lett.* **2014**, *41*, 7276–7283. [CrossRef]
66. Ishii, M.; Kimoto, M. Reevaluation of historical ocean heat content variations with time-varying XBT and MBT depth bias corrections. *J. Oceanogr.* **2009**, *65*, 287–299. [CrossRef]
67. Balmaseda, M.A.; Trenberth, K.E.; Kallen, E. Distinctive climate signals in reanalysis of global ocean heat content. *Geophys. Res. Lett.* **2013**, *40*, 1754–1759. [CrossRef]
68. Willis, J.K. Can in situ floats and satellite altimeters detect long-term change in Atlantic Ocean overtuning? *Geophys. Res. Lett.* **2010**, *37*. [CrossRef]
69. Smeed, D.A.; McCarthy, G.D.; Cunningham, S.A.; Frajka-Williams, E.; Rayner, D.; Johns, W.E.; Meiner, C.S.; Baringer, M.O.; Moat, B.I.; Duchez, A.; et al. Observed decline of the Atlantic meridional overturning circulation 2004–2012. *Ocean Sci.* **2014**, *10*, 29–38. [CrossRef]
70. McCarthy, G.D.; Smeed, D.A.; Johns, W.E.; Frajka-Williams, E.; Moat, B.I.; Rayner, D.; Baringer, M.O.; Meiner, C.S.; Collins, J.; Bryden, H.L. Measuring the Atlantic Meridional Overturning Circulation at 26 N. *Prog. Oceanogr.* **2015**, *130*, 91–111. [CrossRef]
71. Nieves, V.; Willis, J.K.; Patzert, W.C. Recent hiatus caused by decadal shift in Indo-Pacific heating. *Science* **2015**, *349*, 531–535. [CrossRef] [PubMed]
72. Chen, X.; Tung, K.K. Variations in ocean heat uptake during the surface warming hiatus. *Nat. Commun.* **2016**, *7*, 12541. [CrossRef] [PubMed]
73. Liu, W.; Xie, S.-P.; Lu, J. Tracking ocean heat uptake during the surface warming hiatus. *Nat. Commun.* **2016**, *7*, 10926. [CrossRef] [PubMed]
74. Solomon, S.; Rosenlof, K.; Portmann, R.W.; Daniel, J.S.; Davis, S.M.; Sanflord, T.J.; Plattner, G.-K. Contributions of stratospheric water vapor to decadal changes in the rate of global warming. *Science* **2010**, *327*, 1219–1223. [CrossRef] [PubMed]
75. Solomon, S.; Daniel, J.S.; Neely, R.R.; Vernier, J.P.; Dutton, E.G.; Thomason, L.W. The persistently variable "background" stratospheric aerosol layer and global climate change. *Science* **2011**, *333*, 866–870. [CrossRef] [PubMed]
76. Santer, B.D.; Bonfils, C.; Painter, J.F.; Zelinka, M.D.; Mears, C.; Solomon, S.; Schmidt, G.A.; Fyfe, J.C.; Cole, J.N.S.; Nazarenko, L.; et al. Volcanic contribution to decadal changes in tropospheric temperature. *Nat. Geosci.* **2014**, *7*, 185–189. [CrossRef]
77. Kaufmann, R.K.; Kauppi, H.; Mann, M.L.; Stock, J.H. Reconciling anthropogenic climate change with observed temperature 1998–2008. *Proc. Natl. Acad. Sci. USA* **2011**, *108*, 11790–11793. [CrossRef] [PubMed]
78. Hansen, J.; Sato, M.; Kharencha, P.; von Schuckmann, K. Earth's energy imbalance and implications. *Atmos. Chem. Phys.* **2011**, *11*, 13421–13449. [CrossRef]
79. Schmidt, G.A.; Shindell, D.T.; Tsigaridis, K. Reconciling warming trends. *Nat. Geosci.* **2014**, *7*, 158–160. [CrossRef]
80. Kühn, T.; Partanen, A.I.; Laakso, A.; Lu, Z.; Bergman, T.; Mikkonen, S.; Kokkola, H.; Korhonen, H.; Räisänen, P.; Streets, D.G.; et al. Climate impacts of changing aerosol emissions since 1996. *Geophys. Res. Lett.* **2014**, *41*, 4711–4718. [CrossRef]
81. Trenberth, K.E. Has there been a hiatus? *Science* **2015**, *349*, 691–692. [CrossRef] [PubMed]
82. Simmons, A.; Wallace, J.M.; Branstator, G. Barotropic wave propagation and instability and atmospheric teleconnection patterns. *J. Atmos. Sci.* **1983**, *40*, 1363–1392. [CrossRef]

83. Wallace, J.M.; Gutzler, D. Teleconnections in the geopotential height field during the Northern Hemisphere winter. *Mon. Weather Rev.* **1981**, *109*, 784–812. [CrossRef]
84. Folland, C.K.; Parker, D.; Colman, A.W. Large scale modes of ocean surface temperature since the late nineteenth century. In *Beyond El Nino: Decadal and Interdecadal Climate Variability*; Navarra, A., Ed.; Springer: Berlin/Heidelberg, Germany, 1999.
85. Dai, A.; Fyfe, J.C.; Xie, S.-P.; Dai, X. Decadal modulation of global surface temperature by internal climate variability. *Nat. Clim. Chang.* **2015**, *5*, 555–559. [CrossRef]
86. Clement, A.; DiNezio, P. The tropical Pacific Ocean—Back in the driver's seat? *Science* **2014**, *343*, 976–978. [CrossRef] [PubMed]
87. Mantua, N.J.; Hare, S.R.; Zhang, Y.; Wallace, J.M.; Francis, R.C. A Pacific interdecadal climate oscillation with impacts on salmon production. *Bull. Am. Meteorol. Soc.* **1997**, *78*, 1069–1079. [CrossRef]
88. Meehl, G.A.; Hu, A. Megadroughts in the Indian Monsoon Region and Southwest North America and a Mechanism for Associated Multidecadal Pacific Sea Surface Temperature Anomalies. *J. Clim.* **2006**, *19*, 1605–1623. [CrossRef]
89. Huang, R.X. Heaving modes in the world oceans. *Clim. Dyn.* **2015**, *45*, 3563–3591. [CrossRef]
90. Sarachik, E.S.; Winton, M.; Yin, F.L. Mechanisms for Decadal-to-Centennial Climate Variability. In *Decadal Climate Variability*; Anderson, D.T., Willebrand, J., Eds.; Springer: Berlin/Heidelberg, Germany, 1996; pp. 157–210.
91. Wang, C.; Zhang, L. Multidecadal Ocean Temperature and Salinity Variability in the Tropical North Atlantic: Linking with the AMO, AMOC, and Subtropical Cell. *J. Clim.* **2013**, *26*, 6137–6162. [CrossRef]
92. Caesar, L.; Rahmstorf, S.; Robinson, A.; Feulner, G.; Saba, V. Observed fingerprint of a weakening Atlantic Ocean overturning circulation. *Nature* **2018**, *556*, 191–196. [CrossRef] [PubMed]
93. Drijfhout, S.S.; Blaker, A.T.; Josey, S.A.; Nurser, A.J.G.; Sinha, B.; Balmaseda, M.A. Surface warming hiatus caused by increased heat uptake across multiple ocean basins. *Geophys. Res. Lett.* **2014**, *41*, 7868–7874. [CrossRef]
94. Watanabe, M.; Shiogama, H.; Tatebe, H.; Hayashi, M.; Ishii, M.; Kimoto, M. Contribution of natural decadal variability to global warming acceleration and hiatus. *Nat. Clim. Chang.* **2014**, *4*, 893–897. [CrossRef]
95. Douville, H.; Voldoire, A.; Geoffroy, O. The recent global warming hiatus: What is the role of Pacific variability? *Geophys. Res. Lett.* **2015**, *42*, 880–888. [CrossRef]
96. Trenberth, K.E.; Fasullo, J.T.; Branstator, G.; Phillips, A. Seasonal aspects of the recent pause in surface warming. *Nat. Clim. Chang.* **2014**, *4*, 911–916. [CrossRef]
97. Guemas, V.; Douglas-Reyes, F.J.; Andreu-Burrillo, I.; Asif, M. Retrospective prediction of the global warming slowdown in the past decade. *Nat. Clim. Chang.* **2013**, *3*, 649–653. [CrossRef]
98. Meehl, G.A.; Teng, H.; Arblaster, J.M. Climate model simulations of the observed early-2000s hiatus of global warming. *Nat. Clim. Chang.* **2014**, *4*, 898–902. [CrossRef]
99. Bretherton, C.S.; Widmann, M.; Dymnikov, V.P.; Wallace, J.M.; Blade, I. The effective number of degrees of freedom of a time-varying field. *J. Clim.* **1990**, *12*, 1990–2009. [CrossRef]
100. Parker, D.; Folland, C.K.; Scaife, A.A.; Knight, J.; Colman, A.W.; Baines, P.; Dong, B. Decadal and multidecadal variability in the climate change background. *J. Geophys. Res.* **2007**, *112*. [CrossRef]
101. Tung, K.K.; Chen, X.; Zhou, J.; Li, K.-F. Interdecadal variability in pan-Pacific and global SST, revisited. *Clim. Dyn.* **2018**. [CrossRef]
102. North, G.R.; Bell, R.L.; Cahalan, R.F. Sampling errors in the estimation of Empirical Orthogonal Functions. *Mon. Weather Rev.* **1982**, *10*, 699–706. [CrossRef]
103. Bond, N.A.; Cronin, M.F.; Freeland, H.; Mantua, H. Causes and impacts of the 2014 warm anomaly in the NE Pacific. *Geophys. Res. Lett.* **2015**, *42*, 3414–3420. [CrossRef]
104. Hartmann, D.L. Pacific sea surface temperature and the winter of 2014. *Geophys. Res. Lett.* **2015**, *42*, 1894–1902. [CrossRef]
105. Easterling, D.R.; Wehner, M.F. Is the climate warming or cooling? *Geophys. Res. Lett.* **2009**, *36*. [CrossRef]
106. Kostov, Y.; Armour, K.C.; Marshall, J. Impact of the Atlantic meridional overturning circulation on ocean heat storage and transient climate change. *Geophys. Res. Lett.* **2014**, *41*, 2108–2116. [CrossRef]